Electronic Supplementary Information

A Multitude of Modifications Strategy of $ZnFe_2O_4$ Nanorod Photoanodes for Enhanced Photoelectrochemical Water Splitting Activity

Ju Hun Kim[a], Youn Jeong Jang[a],Sun Hee Choi[b], Byeong Jun Lee[a] , Jeong Hun Kim[a], Yun Bin Park[c],

Chang-Mo Nam[d], Hyun Gyu Kim[e] and Jae Sung Lee[a*]*

[a] School of Energy and Chemical Engineering, Ulsan National Institute of Science and Technology (UNIST), Ulsan 689-798, South Korea

[b]Pohang Accelerator Laboratory (PAL), Pohang University of Science and Technology (POSTECH), Pohang 790-784, South Korea

[c]Department of Chemical Engineering, Pohang University of Science and Technology (POSTECH), Pohang 790-784, South Korea

[d]Division of Health and Science, Yeongnam College of Science and Technology, Daegu 705-307, South Korea

[e]Busan Cetre, Korea Basic Science Institute (KBSI), Busan 76742, South Korea

EXPERIMENTAL

Synthesis of ZnFe2O4 nanorod photoanodes by hybrid microwave annealing

The nanostructured ZnFe2O4 photoanode was prepared by a simple solution method. First, as a starting material, amorphous β-FeOOH (akaganeite) nanorods were grown on FTO glass (PECTM 8, 6~9 Ω, Pilkington) at 100 oC using an aqueous solution containing 0.15M FeCl3·6H2O (97%, Sigma Aldrich) and NaNO3 (99%, Sigma Aldrich) for 6 h followed by rinsing with abundant deionized water to obtain yellow colored β-FeOOH thin film. Then 80 μL of 60 mM Zn(NO3)·6H2O (98%, Sigma Aldrich) aqueous solution was added drop-by-drop on the β-FeOOH thin film of 1 cm x 1 cm. For transformation to ZnFe2O4 nanorods, HMA was used instead of high temperature CTA in a muffle furnace. Thus the reactor was filled with 5 g of graphite powder as a susceptor, on which the wetted electrode was loaded and subsequently treated in a home microwave oven at 2.45 GHz, 1 kW for various durations. The microwave treatment turned the β-FeOOH nanorods into ZnFe2O4 nanorods wrapped with excess ZnO surface layer. This ZnO skin was removed by soaking into 100ml of 1M NaOH solution (SAMCHUN) for 12 h with stirring. The procedure resulted in pure ZnFe2O4 nanorods on FTO.

Deposition of TiO2 underlayers

The diluted titanium diisopropoxide bis(acetylacetonate) solution with isopropoxide (75wt% in isopropoxide, Sigma Aldrich) was used to deposit a thin underlayer on the FTO coated glass substrate (PECTM 8, 6~9 Ω, Pilkington) by a spin coating method (3000 rpm for 30 sec), which was then moved to a muffle furnace right away and heated at 250 oC for 30 min. The thickness of TiO2 underlayer on the FTO surface was controlled by dilution with isopropoxide from 10mM to 40mM. The samples with TiO2 underlayer were denoted by the Ti-precursor concentrations like TZF-100mM, etc. The thickness of TiO2 was determined by surface profiler (KLA Tencor, P6)

Hydrogen treatment and co-catalyst deposition.

To form defective oxygen vacancies, the electrodes were subsequently post-treated in a furnace under H2 atmosphere at 200oC for 2 h.

The precursor solution for thin NiFeOx films was prepared by mixing iron (III) 2-ethylhexanoate (50 w/w% in mineral spirits, Sigma Aldrich), nickel (II) 2-ethylhexanoate (78 w/w% in 2-ethylhexanoic acid, Alfar Aesar) and hexanes. Approximately 10μl cm-2 precursor solution was pipetted on a

ZnFe2O4 photoelectrode. The electrode was irradiated with 1sun illumination for 10 min to form NiFeOx and moved to an oven at 100oC for 30 min.2,22

Characterization of the electrodes

X-ray Diffraction (XRD) was carried out on PW3040/60 X'pert PRO machine (PANalytical) with Cu- Kα (λ=1.54056Å) radiation at 40 kV and 30 mA. High-resolution scanning electron microscopy (SEM, HITACHI), scanning transmission electron microscope (STEM, JEOL), X-ray (UV) photoelectron spectroscopy (XPS, UPS, ThermoFisher using Al Kα source) were used to observe the morphology at UNIST Central Research Facilities (UCRF), Ulsan, Korea. The sheet resistnace of thermal treated FTO substrate was measured by the Hall effect measurements (AMP55). The X-ray absorption fine structure (XAFS) measurements were conducted on 7D beamline of Pohang Accelerator Laboratory (PLS-II, 3.0 GeV, 350 mA) in Korea. The radiation was monochromatized using a Si(111) double crystal monochromator. The spectra for K-edges of Fe (Eo=7112 eV) were taken in fluorescence mode at room temperature. The incident beam was detuned by 20% at 7112 eV to attenuate the flux from higher order Brägg diffractions of the silicon crystals. Its intensity was measured with a He-filled IC Spec ionization chamber and the fluorescence signal from the sample was measured with a passivated implanted planar silicon (PIPS) detector. Helium flew continuously into a sample chamber during the measurement so that air scattering of the fluorescence signal should be minimized. Athena and Artemis in the IFEFFIT 1.2.11 suite of software program were used to analyse the obtained data for the local structure study of Fe in ZnFe2O4 photoanodes.

Photoelectrochemical measurements

PEC measurements were performed with a potentiostat (IviumStat, Ivium Technologies) using three electrode cell with the $ZnFe_2O_4$ film, Ag/AgCl (3 M NaCl), and Pt mesh as working, reference, and counter electrodes, respectively. An electrolyte of 1 M sodium hydroxide purged with oxygen-free Ar gas was used for the measurements. All the PEC experiments to obtain photocurrent (I)–voltage (V) curve and EIS were carried out under the one-sun condition ($100mW/cm^2$) by a solar simulator (91160, Oriel) with an AM 1.5G filter. The applied voltage was swept in the range of 0.6–1.7 V_{RHE} with 10 mV/s scan rate. The EIS was measured at a DC potential of 1.23 V RHE and AC potential frequency range 10 000–0.1 Hz with an amplitude of 10 mV. Mott–Schottky analysis was performed by sweeping the range of 0.3–1.7 V RHE with AC frequency of 10 kHz and amplitude of 10 mV under dark condition. The scavenger test for bulk and surface separation efficiency was conducted by adding 100ul of H_2O_2 (30%, Sigma Aldrich) in the 100ml of 1M NaOH solution and followed the

same IV measurement. For the measurement of evolution of hydrogen/oxygen was measured in a closed circulation PEC system with 1cm by 1cm electrodes under 1sun condition at $1.23V_{RHE.}$ For measuring the incident photon-to-current conversion efficiencies (IPCE), a 300Wxenon lamp (Newport, 6258) was coupled to a grating monochromator (Newport, 74125) operating in thewavelength range from 330 to 600 nm, and the incident light intensity was measured with a UV silicon detector (Newport,71675).

Supplementary Note: Hybrid microwave annealing (HMA)

Many ceramic materials at room temperature do not absorb microwaves efficiently because they have poor microwave absorption characteristics (low dielectric constants) that make initial heating difficult. However, once the temperature of material reaches above its critical temperature, microwave absorption becomes efficient to cause self-heating. Here, graphite powder, an excellent microwave absorber, is used as a susceptor. Once the temperature of the graphite powder increases quickly by absorbing microwave, the heat is transferred to the $ZnFe_2O_4$ (ZF) electrode to raise its temperature to the critical temperature. Then, it starts to absorb microwave efficiently.[12,14]

However, it is difficult to directly measure and estimate the temperature of susceptor and the temperature effect of ZF material during this hybrid microwave annealing (HMA). Hence, we compared the properties of XRD between the HMA samples and conventional thermal annealing (CTA) samples. The FWHM values of XRD peaks for the HMA samples were compared with those of CTA samples annealed at 800–1000ºC. In addition, the sheet resistance of those samples was measured and thermal damage of substrate was assessed by naked eyes

The FWHM values of (220) and (311) of HMA samples annealed for 1 - 3 min were similar to those of the CTA sample annealed 1000 ºC. But the sheet resistance of conducting layer (**Table S2**) and appearance of glass substrate (**below**) were preserved only for HMA samples. Therefore we conclude that the ZF could be well crystallized by HMA-2min treatment without degradation of glass and conducting layer

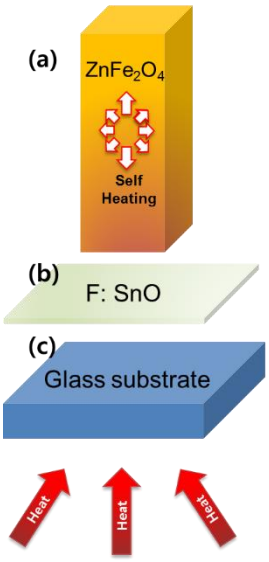

(a)′

XRD peak (FWHM)	HMA (1kW)	CTA (1000ºC)		
	2min	1 min	2min	3min
(220)	0.30	0.50	0.32	0.21
(311)	0.286	0.50	0.29	0.21

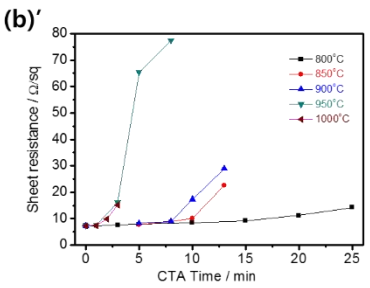

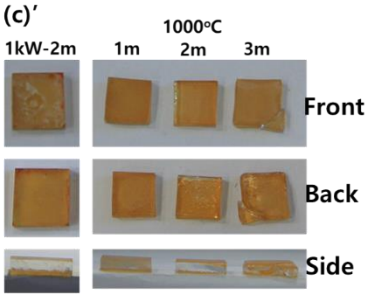

Supplementary Tables

Table S1. Structural parameter calculated from Fe K-edge EXAFS fits for ZF photoanodes prepared by different annealing methods.

	CN[a]	R(Å)[b]	σ^2(Å^2)[c]	R-factor[d]
HMA	6.0	1.993	0.0026	0.0161
CTA	3.3	1.876	0.0052	0.0065
	2.7	2.104		
Standard ZF	6.0	2.104	0.0065	0.0154

[a]Fe-O coordination number (uncertainty < 0.4), [b]Fe-O bond distance (uncertainty < 0.005),
[c]Debye-Waller factor (indicator of the structural disorder, uncertainty < 0.0008),
[d]a-sum-of-squares measure of the fractional misfit.

Table S2. Sheet resistance of FTO annealed by CTA and HMA. Resistances were determined by Hall effect measurements. Here, TiO_2 means that underlayer was spin-coated with the 20 mM Ti precursor solution, then annealed at 250 ºC for 30 min

Samples	FTO (Ω/□)	CTA(Ω/□)		HMA(Ω/□)			
		800ºC-10min	800ºC-20min	2 min	3min	5min	6min
w/o TiO_2	6.3	9.85	12.8	6.5	6.52	9.05	15.2
w/ TiO_2	6.81	10.62	14.5	6.45	6.48	10.8	18.63

Table S3. Structural parameter calculated from Fe K-edge EXAFS fits for ZF/TiO_2/FTO photoanodes

TiO2 concentration	CN[a]	R(Å)[b]	σ^2(Å^2)[c]	R-factor[d]
O mM	6.0	1.993	0.0026	0.0161
10 mM	6.0	2.012	0.0040	0.0123
20 mM	6.0	2.018	0.0050	0.0243
40 mM	6.0	2.031	0.0049	0.0254

[a]Fe-O coordination number (uncertainty < 0.4), [b]Fe-O bond distance (uncertainty < 0.005),
[c]Debye-Waller factor (indicator of the structural disorder, uncertainty < 0.0008),
[d]a-sum-of-squares measure of the fractional misfit.

Table S4. Structural parameter calculated from Fe K-edge EXAFS fits for H_2 treated photoanodes

	CN[a]	R(Å)[b]	σ^2(Å^2)[c]	R-factor[d]
ZF	6.0	1.993	0.0026	0.0161
ZF-H_2	6.0	2.024	0.0014	0.0010
TZF	6.0	2.018	0.0050	0.0243
TZH-H_2	6.0	2.021	0.0049	0.0254

[a]Fe-O coordination number (uncertainty < 0.4), [b]Fe-O bond distance (uncertainty < 0.005),
[c]Debye-Waller factor (indicator of the structural disorder, uncertainty < 0.0008),
[d]a-sum-of-squares measure of the fractional misfit.

Table S5. Relative population of oxygen species derived from deconvoluted XPS O1s peak areas in Figure 5 and Figure S6.

Samples	Relative ratio of O1s peak areas		
	Lattice (O_L)	Vacancy (O_V)	Chemisorb (O_C)
TZF	0.682	**0.137**	0.181
TZF-H_2	0.644	**0.208**	0.148
ZF	0.668	**0.130**	0.203
ZF-H_2	0.650	**0.197**	0.153

Table S6. Comparison of water oxidation performance for single $ZnFe_2O_4$ photoanodes.

Sample description	Support	Synthesis	Photocurrent [mA/cm^2, 1.23V_{RHE}]	Onset potential [V_{RHE}]	Publish Yr.	Reference
Bare	FTO	AACVD	0.35	1.15	2010	1
HMA treatment	FTO	HT / S.C	0.24	0.82	2014	2
H_2 treatment	FTO	HT / S.C	0.32	0.83	2015	3
Inverse opal	FTO, ATO	ALD	0.26	0.9	2016	4
Bare	FTO	CVD	0.085 (1.6V_{RHE})	~1.2	2017	5
Ti doping	FTO	Spray	0.35	0.95	2017	6
Bare	FTO	Electro-spary	~ 0.053	~1.0	2017	7
H2 treatment/NiFeOx cocat	FTO	HT/S.C	~0.36	~0.8	2018	8
Underlayer /Ti doping, /H_2 treatment/ NiFeOx co-cat	FTO	HT/S.C	0.92	0.62		

Note: AACVD (aerosol assisted chemical vapor deposition, HT (hydrothermal), S.C (Solution Casting), ALD (atomic layer deposition), HMA (hybrid microwave annealing)

Reference

1. A. A. Tahir, K. G. U. Wijayantha, *J. Photochem. Photobio. A. Chem.* 2010, **216**, 119-125.

2. J. H. Kim, J. H. Kim, J.-W. Jang, J. Y. Kim, S. H. Choi, G. Magesh, J. Lee, J. S. Lee, *Adv. Energy. Mater.* 2015, **5** 140933.

3. J. H. Kim, Y. J. Jang, J. H. Kim, J.-W. Jang, S. H. Choi, J. S. Lee, *Nanoscale* 2015, **7**, 19144-19151.

4. Y. F. Xu, H. S. Rao, X. D. Wang, H. Y. Chen, D. B. Kuang, C. Y. Su, *J. Mater. Chem. A, 2016,* **4**, 5124-5129

5. D. Peeter, D. H. Taffa, M. M. Kerrigan, A. Ney, N. Jons, D. Roglla, S. Cwik, H-W. Becker, M. Grafe, A. Ostendorf, C. H. Winter, S. Chakraborty, M. Wark, A. Devi, *ACS Sustainable Chem. Eng.* 2017, **5**, 2917-2926

6. Y. Guo, N. Zhang, X. Wang, Q. Qian, S. Zhang, Z. Li, Z. Zou, *J. Mater. Chem. A.* 2017, **5**, 7571

7. M. Wang, Y. Sun H. Chen, Y. Zhang, X. Wu, K. Huang, S. Feng, *CrystEngComm.* 2017, **19**, 772

8. N. Guijarro, P. Bornoz, M. Prevot, X. Yu, Z. Zhu, M. Johnson, X. Jeanbourguin, F. Leformal, K. Sivual, *Sustainalbe Energy Fuels*, 2018, **2**, 103-117

Supporting Figures

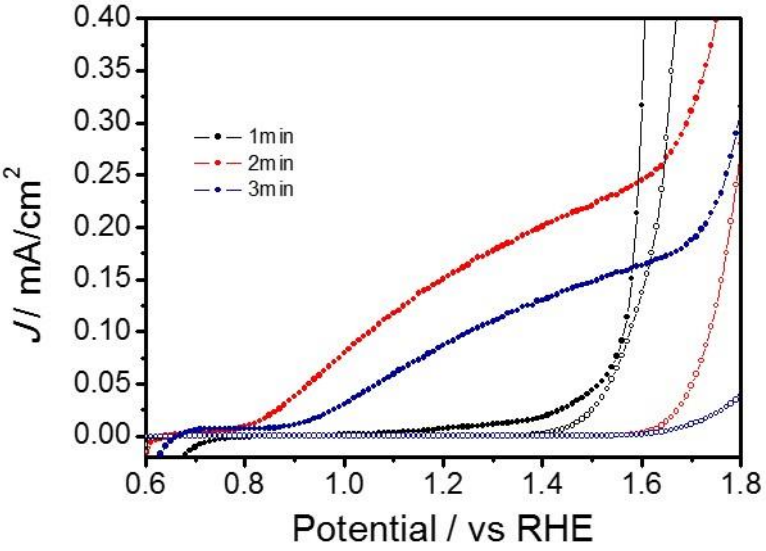

Figure S1. J-V curves for ZF anodes depending on operating time of HMA (1, 2, and 3 min). The measurements were conducted under 1 sun condition in the 1M NaOH solution. (Scan rate: 10mV/s)

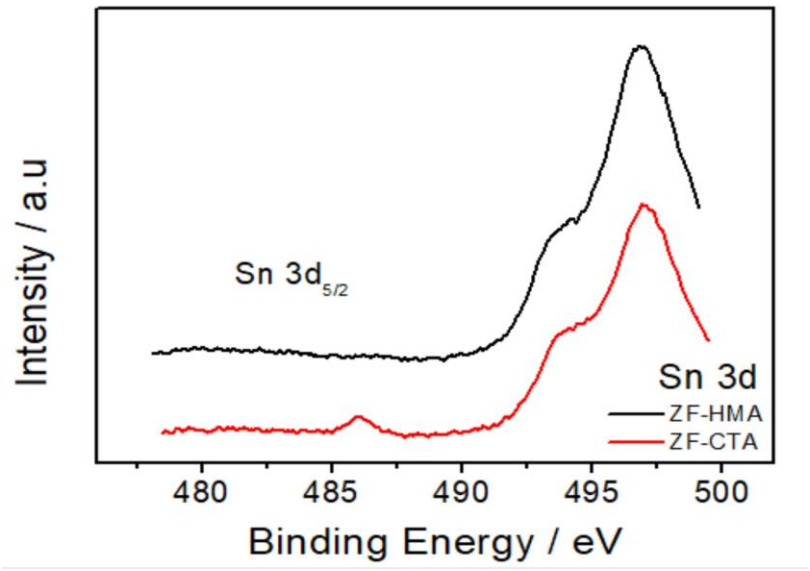

Figure S2. XPS data of Sn for ZF samples fabricated by HMA and CTA. To discuss the presence of Sn, the only lower B.E peak (Sn 3d5/2, 486.2eV) is considered due to overlapped auger peaks of Zn and Na at the higher B.E.

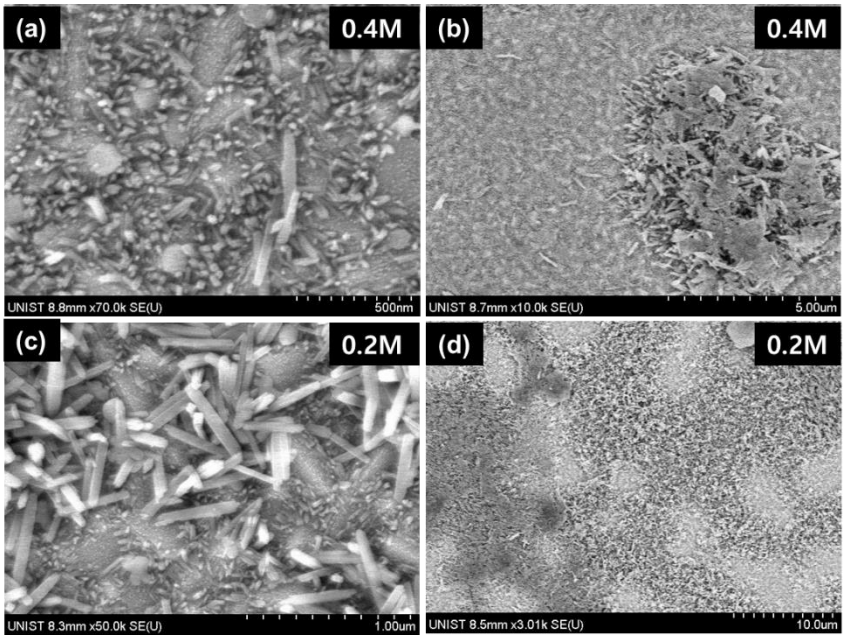

Figure S3. Scanning electron microscopy (SEM) images of FeOOH grown on FTO substrate by hydrothermal synthesis after deposition of TiO_2 underlayer with Ti precursor concentration of 0.4 M (a, b) and 0.2 M (c, d).

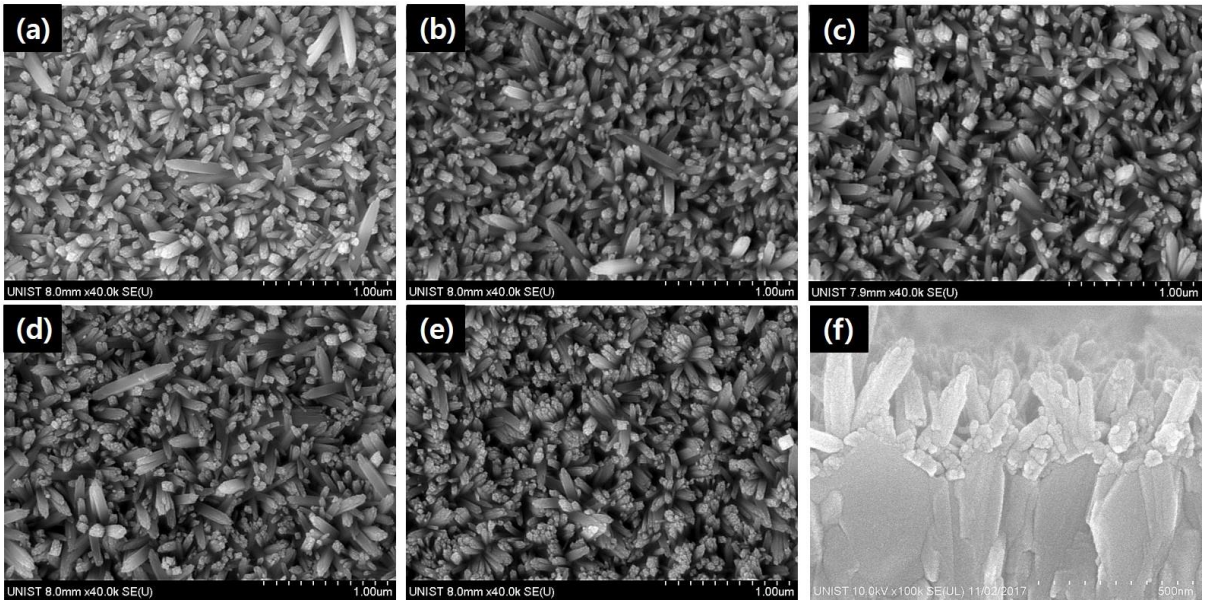

Figure S4. Scanning electron microscopy (SEM) images of FeOOH grown on the TiO_2 underlayer/ FTO substrate by hydrothermal synthesis with different concentration of Ti precursor (a) 100 mM, (b) 40 mM, (c) 20 mM, (d) 10 mM and (e) 5 mM and TiO_2 (20 mM) /$ZnFe_2O_4$.

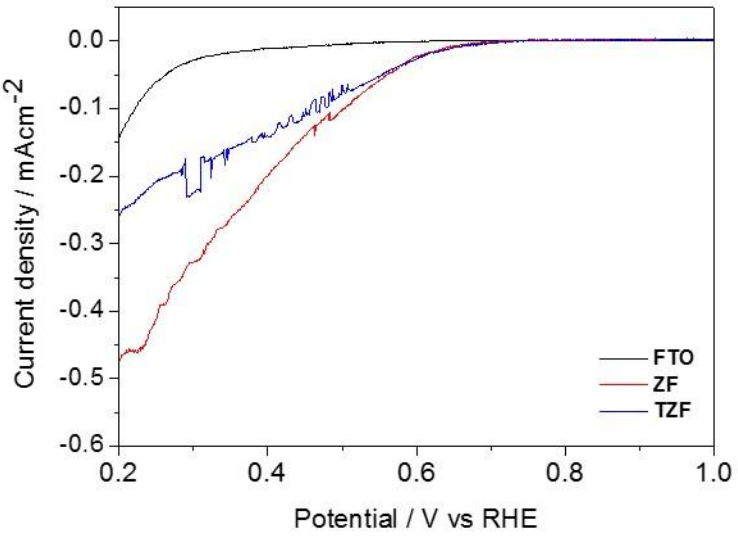

Figure S5. Reduction currents in the dark of FTO, ZF, and TZF in O_2 purged 1 M NaOH.

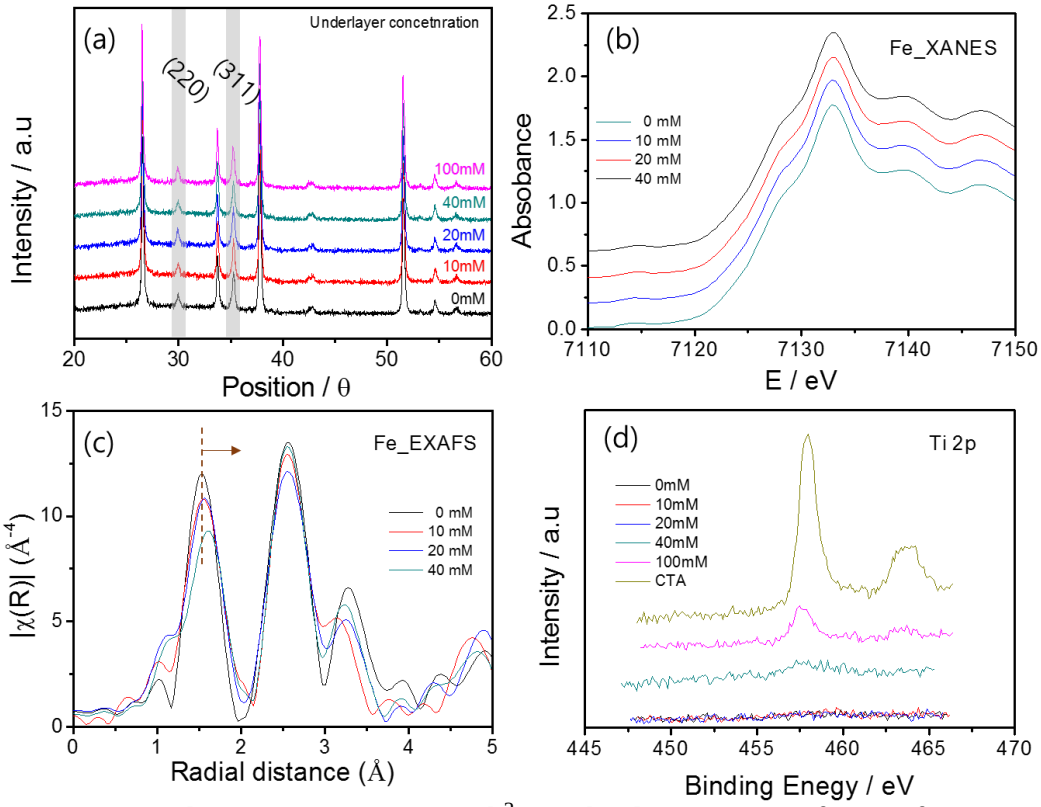

Figure S6. (a) XRD, (b) XANES spectra, (c) k^3-weighted Fourier transforms of EXAFS functions for the Fe K-edges and (d) XPS spectra of Ti 2p of TiO_2 underlayered photoanodes, where CTA denotes the conventional thermal annealing-treated $ZnFe_2O_4$ with 20mM of TiO_2 underlayer.

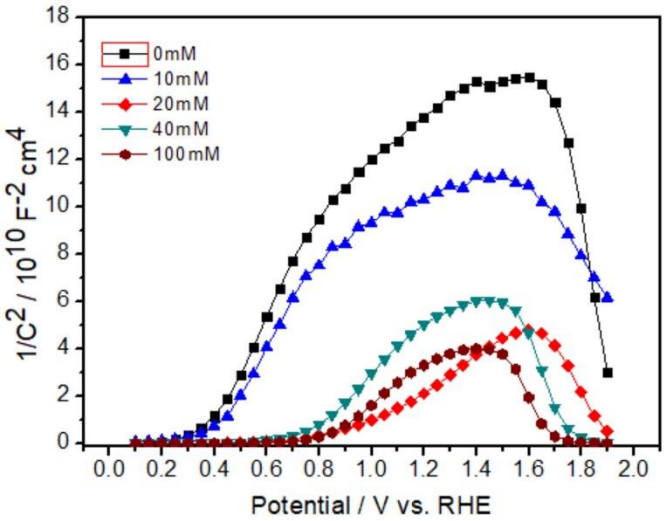

Figure S7. Mott-Schottky plots of TiO_2 underlayered $ZnFe_2O_4$ photoanodes.

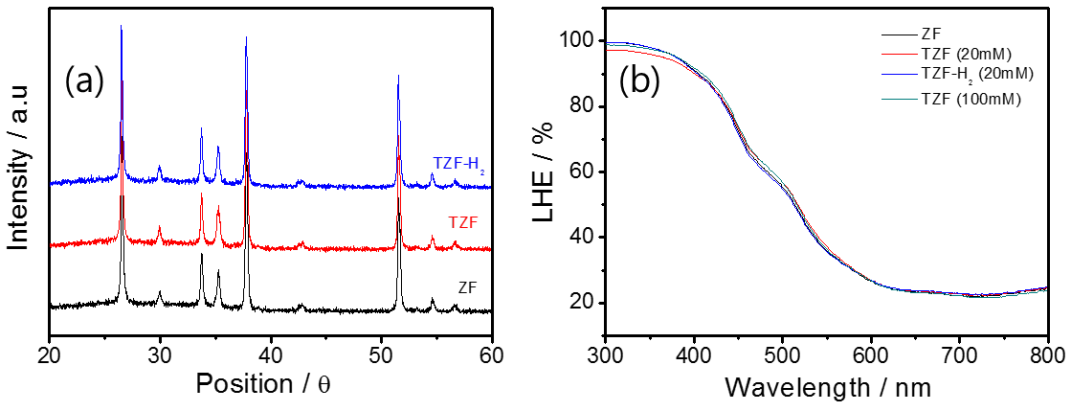

Figure S8. (a) XRD of ZF, TZF (20mM TiO_2) and TZF-H_2 photoelectrodes. (b) Light harvesting efficiency (LHE) of those samples and the 100mM TiO_2 underlayer (the highest concentration) sample.

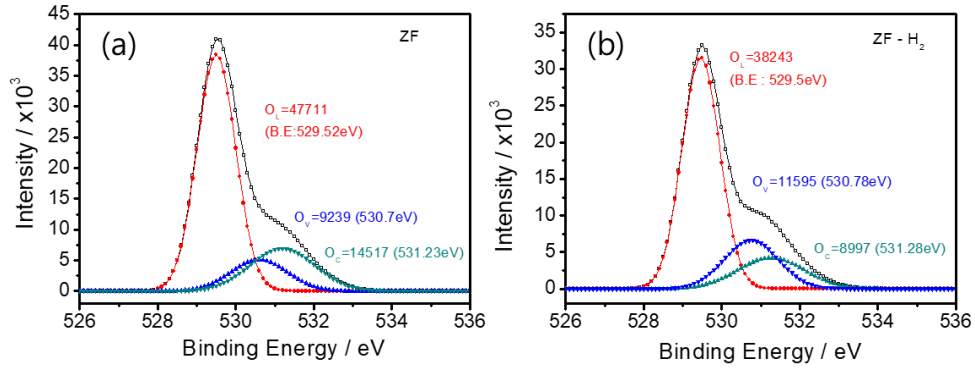

Figure S9. XPS of (a) ZF and (b) hydrogen-treated ZF photoanode, ZF-H_2

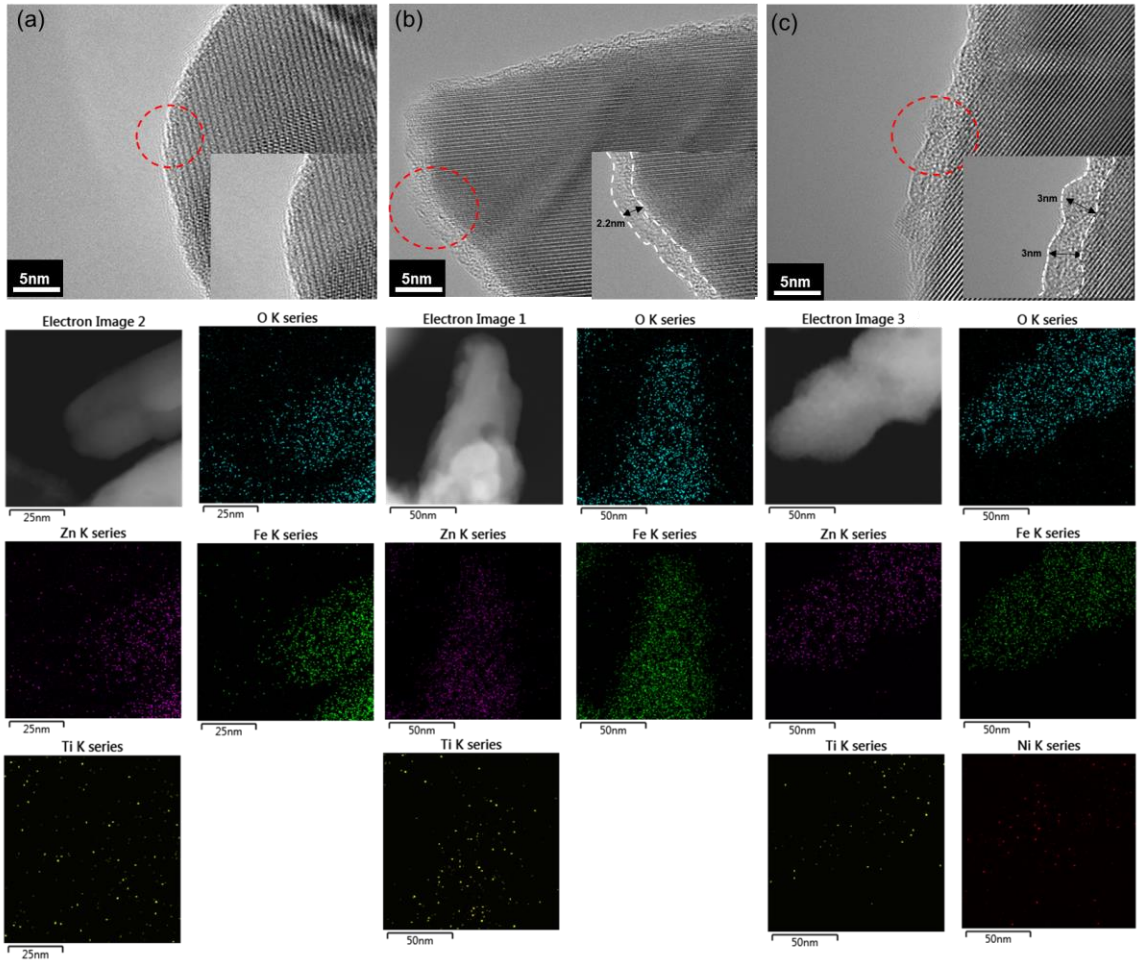

Figure S10. HR-TEM, STEM and EDS data of (a) TZF, (b) TZF-H_2 and (c) NFO/TZF-H_2 photoanodes.

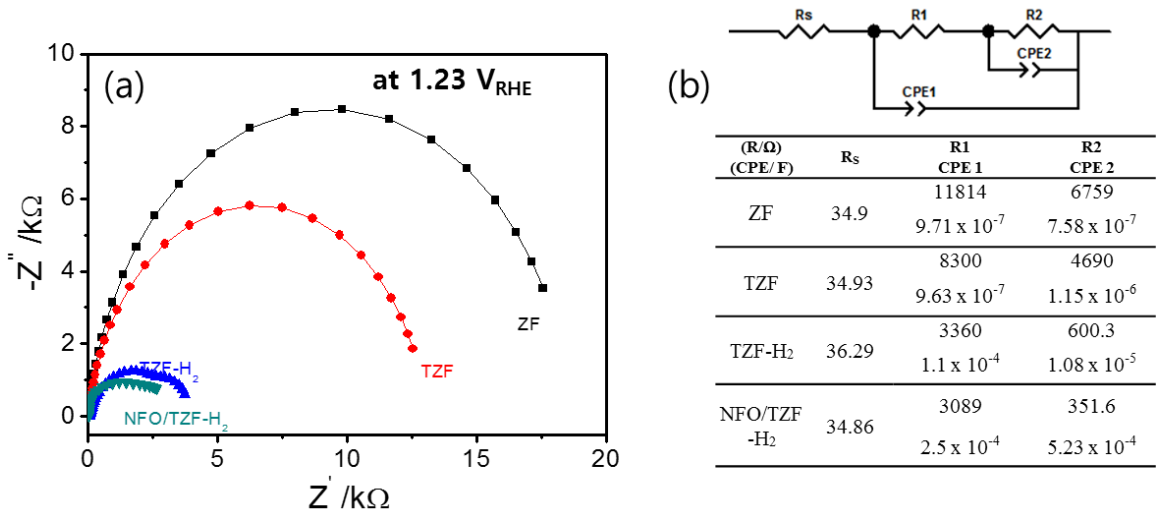

(R/Ω) (CPE/ F)	R_S	R1 CPE 1	R2 CPE 2
ZF	34.9	11814 9.71×10^{-7}	6759 7.58×10^{-7}
TZF	34.93	8300 9.63×10^{-7}	4690 1.15×10^{-6}
TZF-H_2	36.29	3360 1.1×10^{-4}	600.3 1.08×10^{-5}
NFO/TZF -H_2	34.86	3089 2.5×10^{-4}	351.6 5.23×10^{-4}

Figure S11. (a) The Nyquist plots of ZF, TZF and TZF-H_2 photoanodes and (b) the equivalent circuit model used for fitting and fitting results. The EIS measurements were carried out under the one-sun condition at a DC potential of 1.23 V_{RHE} and AC potential frequency range 10 000–0.1 Hz with an amplitude of 10 mV.

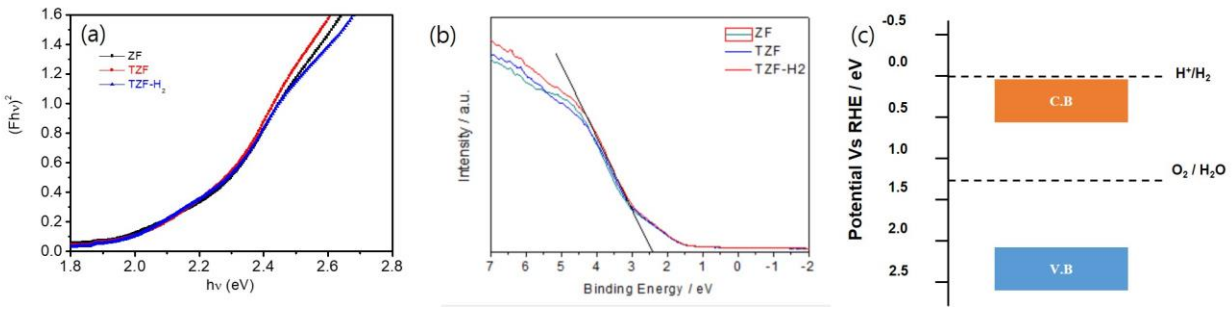

Figure S12. (a) Tauc plots from UV-Vis diffuse spectra based on Figure S8, (b) Ultra-violet photoelectron spectroscopy (UPS), and (c) Schematic band structure of ZF, TZF and TZF-H_2 determined by Tauc plot and UPS. These results show that the multiple modifications do not alter their band structure.

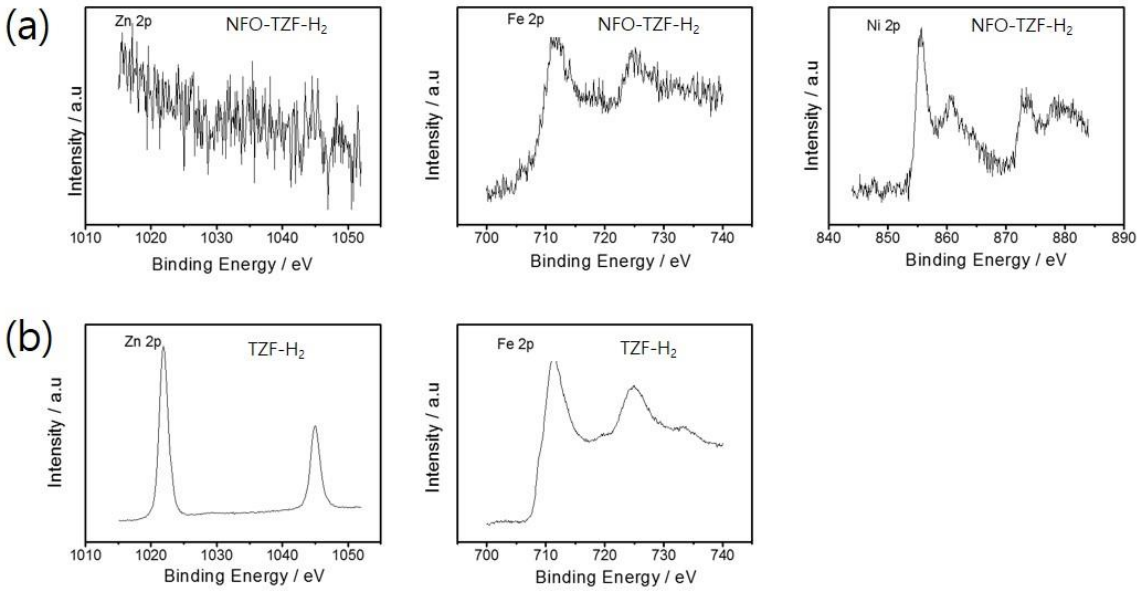

Figure S13. XPS data of (a) NFO/TZF-H_2 and (b) TZF- H_2 photoanode

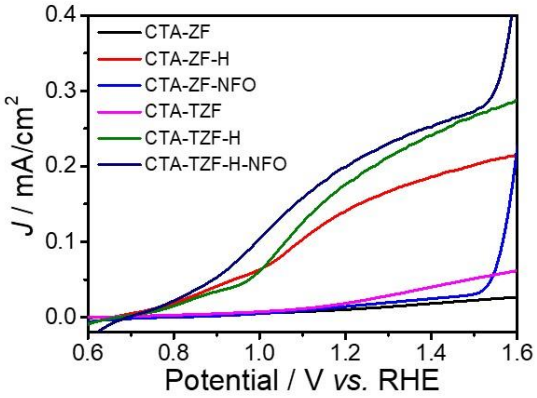

Figure S14. J-V curves of ZF, ZF-H2, TZF, and NFO treated on ZF, TZF, ZF-H_2 and TZF-H_2 fabricated by CTA

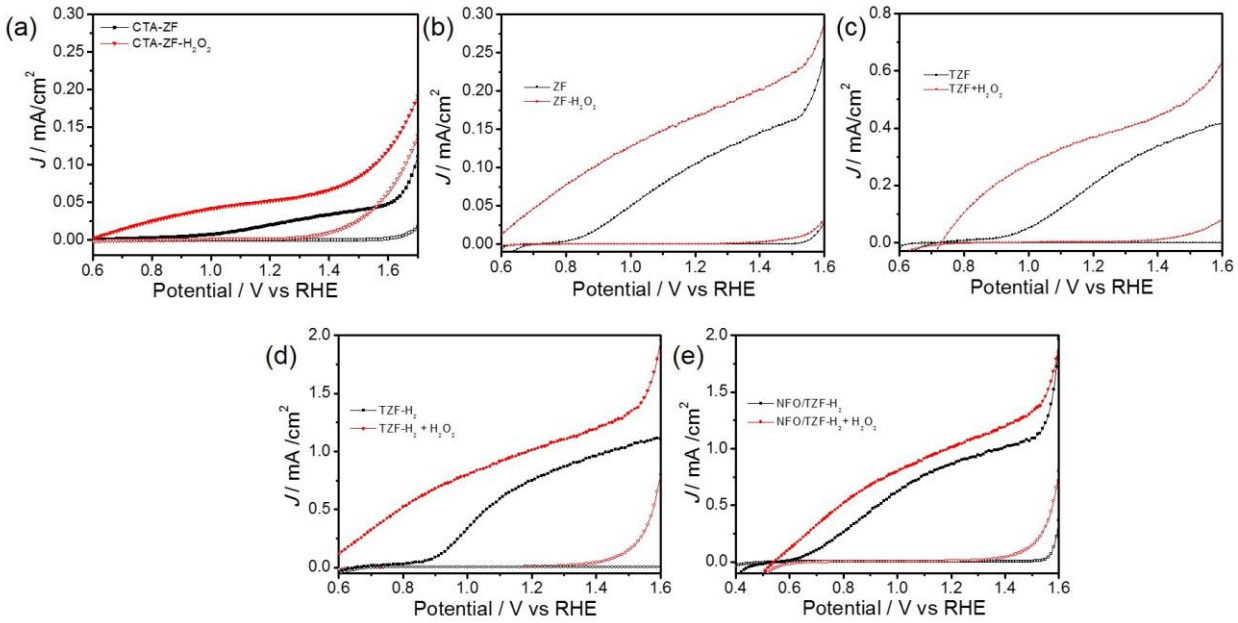

Figure S15. J-V curves of hole scavenger test by adding hydrogen peroxide: (a) ZF (CTA), (b) ZF (HMA), (c) TZF (20mM TiO_2 underlayered $ZnFe_2O_4$), (d) TZF-H_2 (hydrogen treatment on TZF) and (e) NFO/TZF-H_2 (NiFeOx co catalyst loading on TZF-H_2).

$$J_{H2O} = J_{absorbed} \times \eta_{bulk} \times \eta_s \qquad J_{H2O2} = J_{absorbed} \times \eta_{bulk}$$

$$\eta_{surface} = J_{H2O} / J_{H2O2}, \quad \eta_{bulk} = J_{H2O2} / J_{absorbed}$$

$J_{absorbed}$ is the photocurrent density as a result of completely converting the absorbed photons into current. Estimated $J_{absorbed}$ is about 4.27mA/cm^2. In here, absorption data from ZF-HMA) was used, but all of the absorption data are similar with each other.

For calculation of $J_{absorbed}$, correlation between absorbance and radiation proposed by Choi's group was used [1].

$P_d = P_0 10^{-A}$

$P_{abs} = P_0 (1\text{-}10^{-A})$

P_0 (unit: mWcm-2nm-1) is provided power by solar simulator (in this case, AM 1.5G), P_{abs} is power of light actually absorbed by photoanode and P_d is power of light not absorbed to photoanode but dissipated by reflection and penetration. A is absorbance of photoanode (in this case, $ZnFe_2O_4$) and LHE (light harvesting efficiency) is defined as $1\text{-}10^{-A}$. So light which is not absorbed at photoanode will be 10^{-A}. Integrated $P_{abs}(\lambda)$ (mWcm-2nm-1) along with wavelength λ gives total power (unit of mWcm^{-2}), which is power of light absorbed by photoanode (maximum power of photoanode). Below formula shows such relationship photon absorption (Jabs).

$$J_{abs}\left(\frac{mA}{cm^2}\right) = \int_{\lambda_1}^{\lambda_2} \frac{\lambda}{1240} P_{abs}(\lambda) d\lambda \quad \left(\frac{mW}{cm^2}\right)$$

The bulk separation value was calculated with J_{abs} is of ~ 4.27 mA/cm^2 till 2.1 eV threshold.

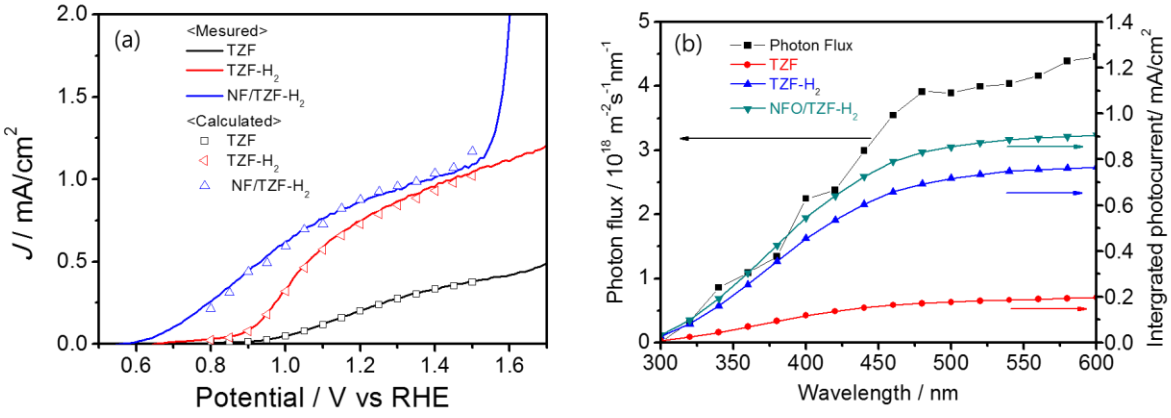

$$J = J_{abs} \times \eta_{bulk} \times \eta_{surf} \times \eta_{F.E}$$

$$J = \int_{300}^{600} \frac{1}{1240} \lambda \, IPCE(\lambda) E(\lambda) d(\lambda)$$

Figure S16. (a) the comparison of the measured and calculated photocurrent density. The faradaic efficiency ($\eta_{F.E}$) is considered as a unit. (b) Integrated photocurrent based on the IPCE data (300-600nm) collected at 1.23V vs RHE and the standard photon flux is shown.

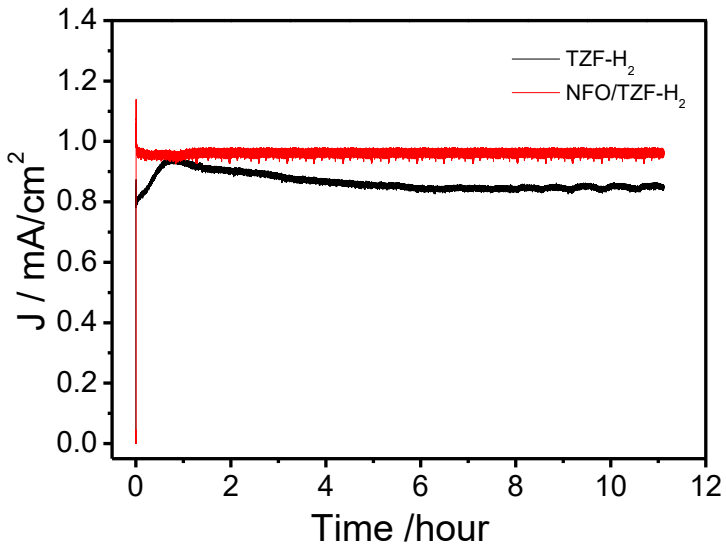

Figure S17. The stability test of TZF-H_2 with and without $NiFeO_x$ co-catalyst under 1sun condition at 1.23 V_{RHE}.

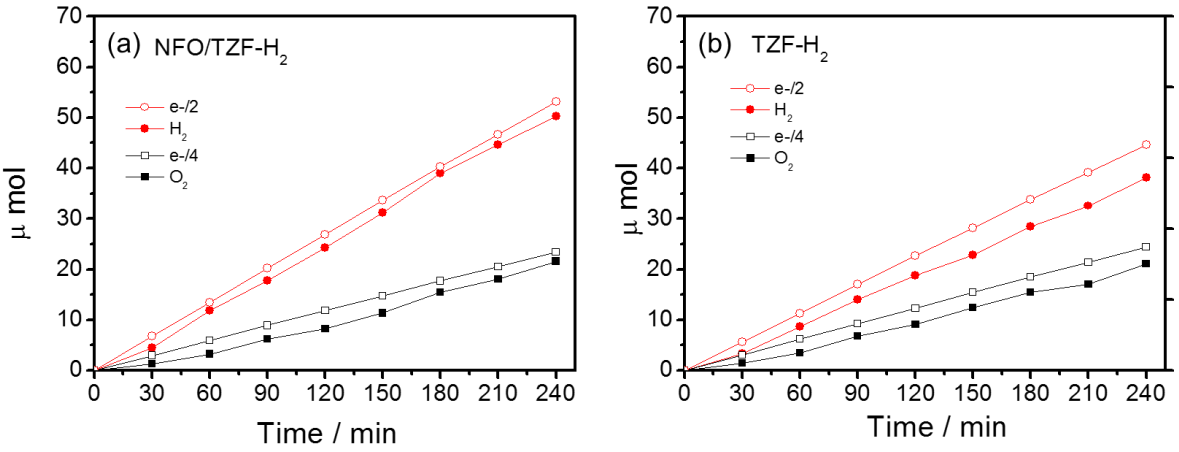

Figure S18. Evolution of hydrogen /oxygen from the NFO/TZF-H_2 and TZF-H_2 photoanodes are compared with the theoretical gas evolution deduced from photocurrent. The evolved hydrogen/oxygen gases measured in a closed circulation PEC system with 1cm by 1cm electrodes under 1sun condition at $1.23V_{RHE}$.